JOURNAL OF SPACECRAFT AND ROCKETS
Vol. 31, No. 4, July–August 1994

Optical Properties of Orbital Debris

Karl G. Henize* and Christine A. O'Neill†
NASA Johnson Space Center, Houston, Texas 77058
and
Mark K. Mulrooney‡ and Phillip Anz-Meador§
Lockheed Engineering and Sciences Company, Houston, Texas 77058

This paper discusses the albedos and phase angle effects found for 400 members of seven debris swarms using observations obtained in 1990 and 1991 with the NASA Johnson Space Center charge couple device-equipped portable Schmidt telescope. The mean albedo derived by comparing optical brightnesses with averaged radar cross sections (RCSs) is 10%. The standard deviation in log albedo is 0.35 if the RCSs are assumed to contribute equally to the scatter. Forty objects are sufficiently free of tumble or aspect angle effects to yield consistent phase function slopes. These range from specular in nature (zero slope) through lambertian (moderate slope) to lunar (steep slope) with the mean lying midway between specular and lambertian. Swarm-to-swarm comparison shows the Cosmos 1375 debris to have unusually small scatter in albedo and the Spot 1/Viking debris to have unusually bright albedos.

Nomenclature

A = Bond albedo
a = solar phase angle
B = blue magnitude
d = distance of satellite, km
F = fraction of incident flux that reaches the observer
G = value of normalized phase function at 90-deg solar phase angle
M = absolute magnitude
m = apparent magnitude
r = radius of satellite, cm
s = slope of adopted linear phase function
U = analog-to-digital units
V = visual magnitude
ϕ = phase function, flux per unit solid angle $\times \Pi$

Introduction

THE Space Sciences Branch of the NASA Johnson Space Center (JSC) is carrying out a program to measure the optical properties of known particles of orbital debris. Such information as the characteristic value of the Bond albedo and the dependence of brightness on phase angle is fundamental in interpreting the data obtained by optical systems searching for new debris. Debris from seven breakups (Cosmos 1275, Cosmos 1375, Landsat 1, Landsat 3, NOAA 3, Nimbus 4, and Spot 1/Viking) has been observed yearly since 1987.

Early observations were made with a 20.3-cm aperture optical system from the Lenzar Optics Corporation equipped with an intensified vidicon detector. Beginning in 1989 observations were obtained with a telescope equipped with a charge couple device (CCD), which is described later. The CDT data from the CCD-equipped telescope have significantly greater photometric accuracy, and when operated in the time-delayed integration (TDI) mode during the 1990 and 1991 observing seasons, the CDT recorded objects with radar cross section (RCS) values as small as 0.01.

Before 1987 a value of 0.5 was commonly assumed for the Bond albedo of space debris. However, early observations acquired with the Lenzar telescope[1] indicated a mean albedo less than 0.1 and showed that the mean albedos for some debris swarms were systematically higher or lower than for other swarms. At about the same time Henize and Stanley,[2] analyzing photometrically calibrated data from telescopes of the U.S. Air Force ground-based electro-optical deep space surveillance network (USAF GEODSS), found a mean albedo of 0.08.

The aforementioned albedos were obtained by comparing the optical brightness with the RCS. It is of interest to compare these values with albedos obtained by comparing optical and infrared brightnesses. Studies of this type using data from the USAF Maui optical station were initiated by the Johnson Space Center. A preliminary study[3] included 13 objects and found albedos ranging from 0.01 to 0.18 with 11 objects having albedos less than 0.1. A subsequent analysis of these observations sponsored by the USAF Phillips Laboratory using a different thermal model showed a wide range of albedos with a median of 0.14.[4]

The aim of the present paper is to give the results obtained from CDT observations of 400 objects in 1990 and 1991.

Observations

The observations reported here were obtained in 1990 and 1991 with a CCD-equipped, 31.8-cm, f/1.3 Schmidt telescope located for two weeks each year at the Rattlesnake Mountain Observatory of the Battelle Pacific Northwest Laboratories near Richland, Washington. The telescope and its operating modes have been described more completely by Henize et al.[5] All data were obtained using the TDI operating mode that allows effective exposures on the order of 4–6 s. In 1990, objects with RCSs less than 0.10 were excluded from the target list, but this limit was dropped in 1991. For objects with cataloged RCSs of 0.01, a success ratio greater than 50% was achieved.

It was a basic aim to obtain two observations of each object at an interval of 80 s (we refer to these as "phase angle pairs") to get phase function information. However, time overlap problems frequently allowed only one observation of a given object. The limit of two observations per satellite was set mainly by the fact that telescope pointing was performed manually. A

Presented as Paper 93-0162 at the AIAA 31st Aerospace Sciences Meeting, Reno, NV, Jan. 11–14, 1993; received March 3, 1993; revision received July 13, 1993; accepted for publication July 23, 1993.

*Senior Scientist, Space Sciences Branch.
†Space Scientist, Space Sciences Branch.
‡Senior Associate Scientist.
§Principal Scientist.

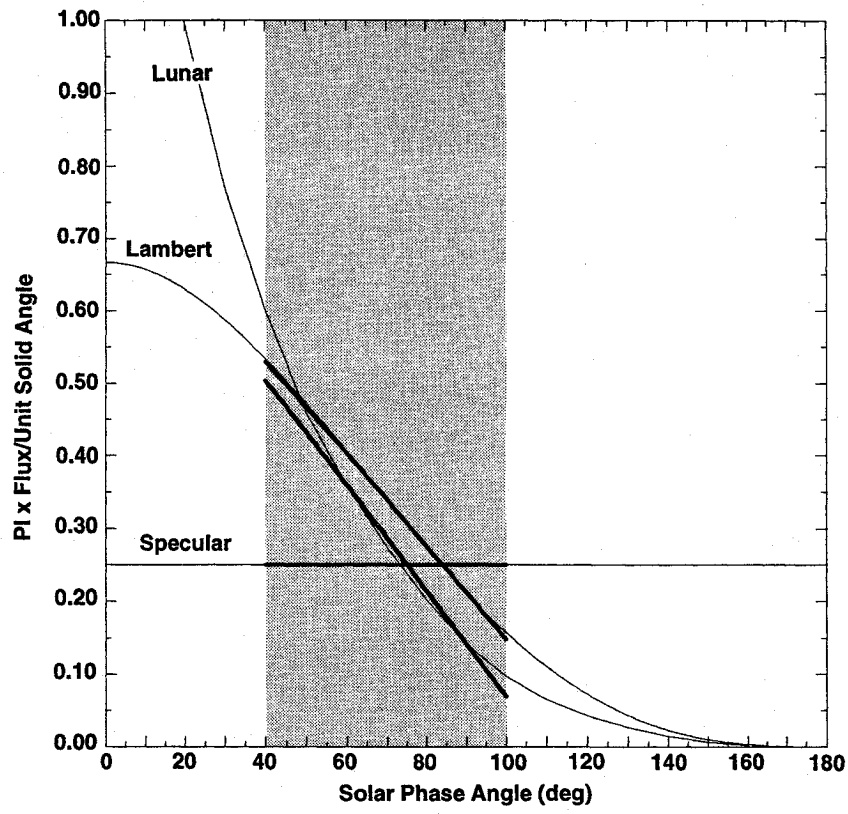

Fig. 1 Three representative phase functions.

Table 1 Observation statistics

Obs. or Pairs/ Object	Frequency	
	Obs.	Pairs
1	101	182
2	121	57
3	71	15
4	56	2
5	22	0
7	7	0
8	6	0
9	2	0
10	0	0
11	1	0
Total	1094	349

computer-controlled mount was acquired in early 1992 and allows up to eight observations per satellite pass. Observations obtained in 1992 are still being analyzed and will be reported in a later paper.

A total of 1230 positive observations of 421 objects was obtained during the 1990–91 observing seasons. After all images acquired under questionable cloud conditions are eliminated, 1094 observations of 400 objects remain. These include a total of 349 phase angle pairs. Table 1 gives an account of the multiplicity of observations and phase angle pairs per object; e.g., 121 objects were observed twice and 57 objects had two phase angle pairs.

Photometry

Observations of one or more standard photometric sequences were made several times per night. These are used to monitor sky transparency and to calibrate the CCD. The resulting calibration equation is

$$m = 17.5 - 2.5 \log U \tag{1}$$

Since no filters were used, this instrumental magnitude is biased toward the red end of the spectrum by the CCD spectral sensitivity. The color equation for the CCD-telescope combination obtained from the photometric sequences is

$$m = V - 0.6\,(B - V - 0.65) \tag{2}$$

where 0.65 is the B-V color of the sun. Thus m is the equivalent of the V magnitude for objects with the color of the sun, a condition that is approximately true for satellites illuminated by the sun. Thus no color correction is applied to satellite observations.

The apparent magnitude m of a satellite is obtained by dividing the analog-to-digital count of the integrated image by the field crossing time (i.e., the exposure time in seconds) and entering this into Eq. (1). The absolute magnitude is obtained by correcting apparent magnitude to a standard distance of 1000 km and to a solar phase angle of 90 deg. Thus,

$$M = m - 5 \log (d/1000) + 2.5 \log [1 + s(90 - a)] \tag{3}$$

Equation (3) assumes the phase function to be linear. The degree to which this is true over the 40–100 degree phase angle range in which nearly all of the observations fall is shown in Fig. 1, which illustrates the three phase functions—specular, lambert, and lunar—chosen to represent the variety of slopes evident in our data. Only the lunar function departs appreciably from linearity in the region of practical interest indicated by the stipled area in Fig. 1. The lunar phase function used here is based on empirical data given by Allen.[6]

The adopted linear approximations to the phase functions may be expressed by the following equation:

$$\phi = G\,[1 + s(90 - a)] \tag{4}$$

with constants as given in Table 2.

For "well-behaved" objects (i.e., those that do not show large brightness variations due to their irregular shape), the phase function slope for each object may be derived from the observations when one or more phase angle pairs are available (see the following section titled Phase Functions). For the remainder,

Table 2 Constants for three representative phase functions

Type	G	s
Specular	0.250	0.000
Lambert	0.212	0.030
Lunar	0.142	0.051

a mean slope of 0.015, the mean for the well-behaved objects, has been applied.

The derivation of absolute magnitudes is necessary when combining several observations for one object to eliminate the effects of varying distances and phase angles before determining a mean or median value for the object. The scatter in absolute magnitudes may be considered a measure of the irregularity of the object. The absolute magnitudes are also the most direct quantity to be used in comparing the results of various optical observers.

When the absolute magnitude is used to derive the Bond albedo (or to derive a particle diameter assuming an albedo), we must also apply a normalizing factor G required to reduce the integral of the phase function to unity. This factor is the value of the normalized phase function at a 90-deg phase angle (see Fig. 1) and is derived by interpolating between the known values for the three "standard" phase functions by comparing the observed slope with the slopes of the standard functions.

Having derived a value for G (or by assuming a mean value related to the mean slope), we may then calculate a Bond albedo for objects for which either true dimensions or RCSs are available:

$$A = F/r^2G \tag{5}$$

where

$$F = 10 \exp[0.4\,(-26.74 - M)] \tag{6}$$

where -26.74 is the absolute visual magnitude of the sun. It should be noted that a factor of pi, which might be expected to appear in Eq. (5), has been absorbed into the value of G.

Conversely, by assuming an albedo (e.g., the median value derived in the following section), Eq. (5) may be used to derive the radius of newly discovered objects.

Albedos and Diameters

In the following, albedos are derived by comparing the absolute magnitudes with RCS data obtained from the U.S. Space Command. A major effort has been made to reduce the scatter found in month-to-month RCS values by combining the data found in 47 RCS catalogs obtained between 1977 and 1992. After default values and values repeated without update are eliminated, the medians and means of the remaining RCS values are derived. Perusal of the data shows the frequent occurrence of spuriously high values that may differ by an order of magnitude or more from the bulk of the data points. For this reason we have chosen the median values for the albedo calculation since medians are less affected than means by these spurious values.

Previous work has shown that the published RCS values are too large by a factor of roughly two.[7,8] On examining the systematic trends in the 47 catalogs, we find three distinctly different calibration factors depending on the date.[9] The RCSs used here have been corrected by these factors accordingly.

Because the scattering efficiencies of objects in the Mie and Rayleigh regions differ substantially from the geometrical optics region, the RCS values must be corrected appropriately to reflect the true physical cross section of the target object. A NASA-sponsored program of radar laboratory measurements of orientation/frequency dependencies of debris objects has produced statistical correction factors that are utilized herein.[10] These corrected cross sections are then utilized in obtaining the albedo.

Apparent magnitudes and RCSs corrected as noted earlier have been used to obtain the Bond albedo implied by each observation. The logarithmic distribution of albedo for all 1094 observations is shown in Fig. 2. The median value lies at -1.05 corresponding to a median albedo of 8.9%. The fact that 24 observations have impossible values greater than 1 may be attributed either to anomalies in the optical data such as specular flashes or to problems in the RCSs due to either geometrical or compositional effects. The fact that 8 of the 24 high values have brightness values more than a factor of 3 greater than the next brightest observation for the object lends credence to the specular flash hypothesis. On the other hand, it is clear that the RCS values may frequently be deviant by factors of 2 or more and that this also contributes significantly to the scatter seen in Figs. 2 and 3.

It is useful to know the expected standard deviation about the median albedo when true diameter distributions are being derived from a set of optically derived diameters. The data in Fig. 2 give a standard deviation of 0.50 in log albedo that implies that 67% of the observations lie within a factor of 3.2 of the median value. If we assume that this scatter may be apportioned equally between albedo and RCS, we divide the combined standard deviation by $\sqrt{2}$ to find the standard deviation of either parameter. This gives a standard deviation in log albedo of 0.35; i.e., 67% of the observations would lie within a factor of 2.2 of the median value. It may be expected that these results also apply to the scatter seen in Fig. 3.

It must be noted that the median albedo depends slightly on the assumed phase function. The previous data assume a hybrid phase function lying midway between lambert and specular. In the extreme case of zero slope in the phase function (the specular case), brightnesses and hence albedos are increased, and we find a median albedo of 11.2%.

A useful graphical display of the scatter in these data is shown in Fig. 3 where the log of the optical diameter based on an assumed median albedo of 0.10 is plotted vs the log of the radar-derived diameter. Objects lying on the center 45-

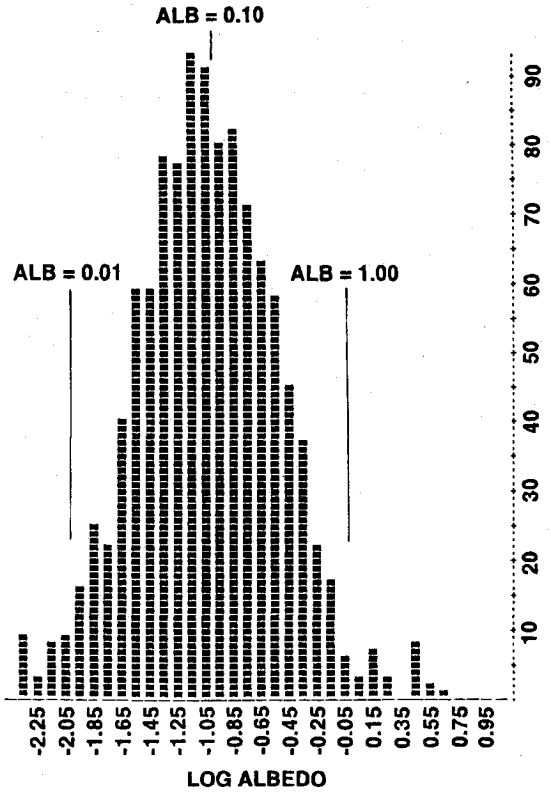

Fig. 2 Distribution of albedos for 1094 observations.

deg diagonal have identical optical and radar diameters, which indicates the assumed albedo is correct. Objects to the right either have anomalously small RCSs or else have albedos greater than the assumed value. If we assume errorless RCSs, we may thus interpret left-right shifts as albedo changes. Following this concept, the locus of albedo values of 1.0 and 0.01 are also indicated in the plot.

Figure 3 shows one point per object for each of 288 objects. Objects of low weight (only one optical observation or less than three radar observations) have been eliminated. The plot illustrates the generally good correlation between optical and radar diameters. The most deviant objects are the three far to the right of the line for albedo = 1.0. In the order of decreasing radar diameter these are Space Surveillance Center catalog numbers 17110, a Spot 1/Viking fragment; 4637, a Nimbus 4 fragment; and 2909, the spherical calibration satellite Surcal 150B.

For the first two objects it might be suspected that the high albedos are the result of specular flashes off flat surfaces on the object, but there is no evidence of this in the optical data. Both have two observations that are in good agreement. The third object, 2909, is an interesting example of the spherical calibration satellites, several of which were included in the 1991 observing program. These are objects of known dimensions that should be free of brightness variations due to irregular shapes or varying aspect angles. All have been in orbit for many years, and although little is known about the current physical state of the aluminum surfaces, it would not be unreasonable to expect diffusely reflecting surfaces with albedos on the order of 50% or greater.

A special study has been made of albedos based on the true physical dimensions of five such objects observed in 1990–91. The albedo of 2909 based on three observations is 66%. Other objects in this study include 900 Calsphere 1 (one observation only) with an albedo of 93%, 902 Calsphere 2 (four observations through thin clouds and thus excluded from the present data) with an albedo of 85%, 5398 LCS 4 (two observations, included in the present data with an RCS-based albedo of 77%) with an albedo of 81%, and 2872 Surcal 159 (seven observations, included in the present data with an RCS-based albedo of 9.8%) with an albedo of 18%. A significant scatter in 2872 absolute magnitudes suggests that it is not spherical and that it may not be the actual calibration sphere.

The albedos for the calibration spheres lend credibility to the calibration of our photometry and thwart potential skepticism concerning the unexpectedly low value for the median albedo of the debris objects.

It would not be completely unexpected to find that the albedo varies with the size of the object. Figure 3 suggests that a marginal effect of this type exists. The objects with diameters greater than 1 m tend to fall to the right of the median line, whereas objects in the 10–20-cm diam range appear to veer slightly to the left of the median line. However, the latter effect is very probably due to the proximity of the sharp cutoff near 12 cm in the corrected radar diameters. If it were real, it would imply that the smaller debris particles have albedos significantly less than the assumed median value.

Phase Functions

For those objects with two or more phase angle pairs, we obtained a phase function slope by averaging the pairs. Converting fluxes to logarithms before calculating the slope obviated the problems associated with systematic night-to-night or year-to-year baseline differences. These slopes were then used to correct each data point to a phase angle of 90 deg. Of the 74 objects for which this was done, 57 had sufficiently small scatter in the corrected brightness (<0.3 magnitude) to be considered well represented by the determined phasefunction.

By reference to three common descriptor phase functions—the perfectly reflecting sphere, the perfectly diffusing (lambert)

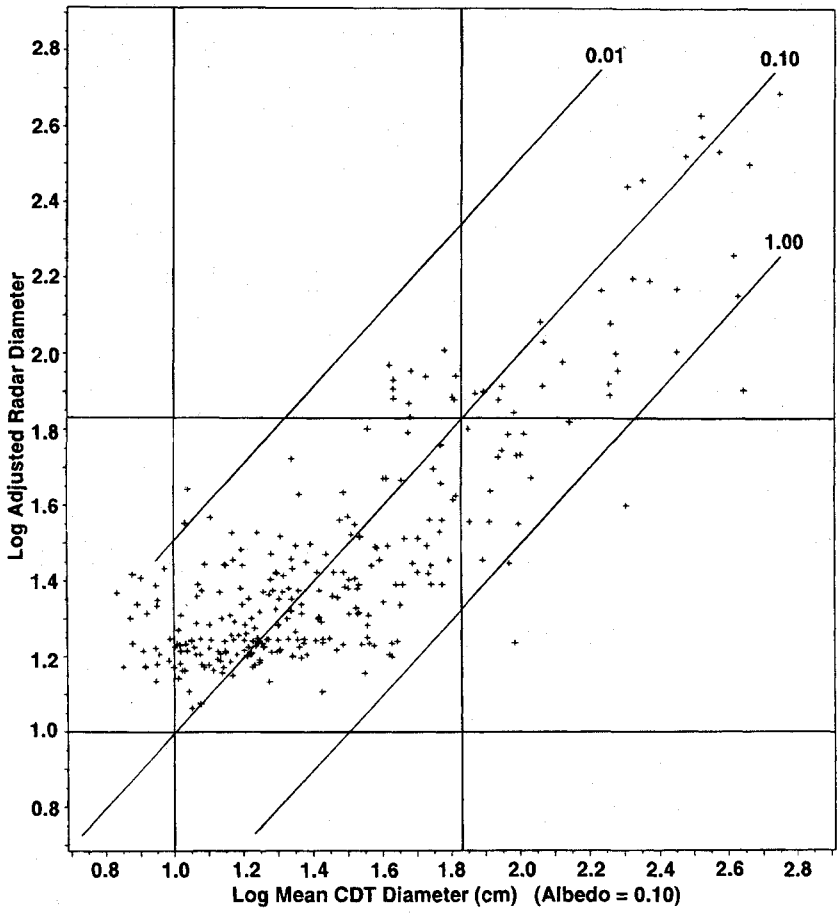

Fig. 3 Optical vs radar diams for 288 objects.

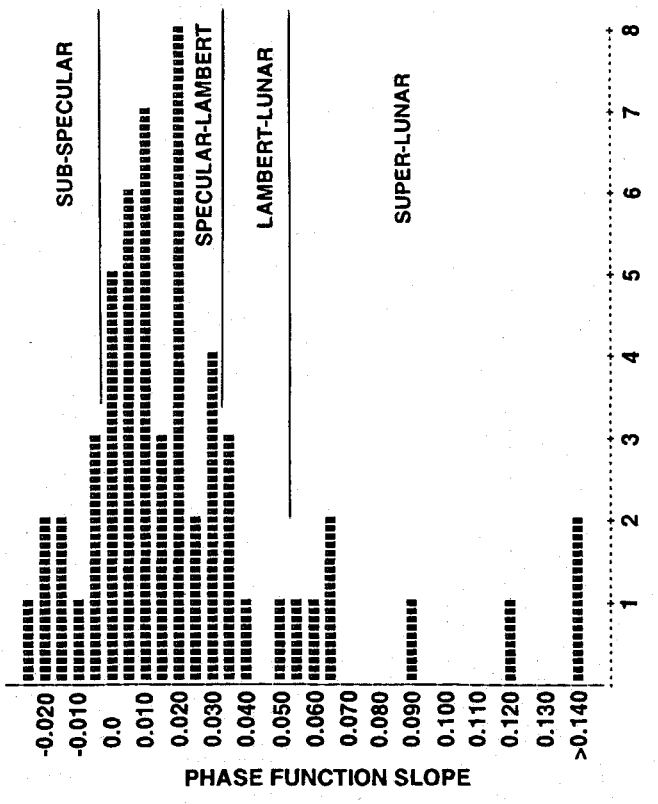

Fig. 4 Distribution of phase function slopes for 57 objects with two or more consistent slopes.

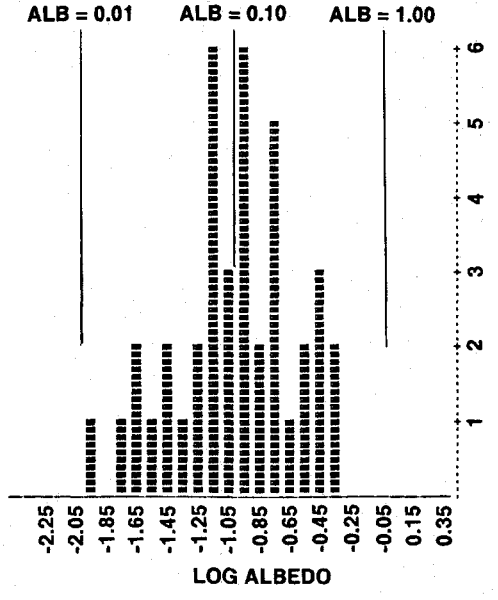

Fig. 5 Distribution of albedos for 40 objects with well-determined phase functions.

sphere, and the moon (see Fig. 1)—it is evident that the observationally derived slope uniquely determines a hybrid phase function that can be expressed in terms of a linear combination of the fully normalized descriptor functions. The derived mixing ratio may be regarded as a possible indicator of surface texture with a smooth transition from the polished specular sphere to objects with the deep pitting and cratering of the lunar surface.

It might seem that deriving phase functions for irregular objects from reference functions based on spheres is overly simplistic. However, with a sufficient number of observations it may be hoped that a statistically valid result will be obtained. It seems logical that an empirically derived mean phase function should be more suitable for analyzing observations than any one theoretical function such as the commonly used lambert function.

Figure 4 shows the distribution of phase function slopes. Of the 57 objects, 40 fall in the specular to lunar range. This leaves 17 objects outside this "normal" range. These peculiar objects are divided into two groups: the subspecular (SS) and superlunar (SL). The nine members of the SS group are extraordinary in that, contrary to common logic, they brighten with increasing solar phase angle. It must be speculated that these are irregular objects stabilized in a way such that they persistently present a larger apparent cross section at the larger phase angles. A similar (but inverted) hypothesis may also be invoked to explain the superlunar objects, but in this case it is also possible that the unusually steep slopes are due to an extreme degree of pitting and/or scoring. However, the fact that 16% of the original 57 objects require a hypothesis based on stabilization raises the logical question as to what degree are the normal phase function slopes controlled in this way. This is an interesting area for future investigation.

The median phase function slope derived from all 57 objects is 0.015, midway between specular and lambert.

The absolute magnitudes and the associated Bond albedos obtained for these objects with individually determined phase functions should be significantly more reliable than the values obtained using only a median phase function as was done in the previous section. Thus it is of interest to compare their albedo statistics with those for the total population.

Figure 5 shows the distribution of derived albedos for the 40 objects with phase functions falling in the normal range. The median value is 10.5%, slightly greater than the value of 8.9% determined for the total population. The standard deviation of log albedo is 0.30, a value that includes the effect of RCS scatter as well as albedo scatter. This is a substantial reduction from the standard deviation of 0.50 found for the total population in Fig. 2.

Figure 6 shows the log-log plot of radar diameter vs optical diameter for these objects based on the 10.5% albedo. It is evident that the scatter is significantly less than the scatter observed in Fig. 3.

Swarm-to-Swarm Differences

It is of interest to investigate swarm-to-swarm differences in albedo. It might be hoped that with sufficient data such differences might give a clue as to cause of particular breakups. Log-log plots of radar vs optical diameters were examined for all seven swarms. Most swarms mimicked the general trend and scatter seen in Fig. 3 for the total set of objects. However, two swarms—Cosmos 1375 and Spot 1/Viking—showed a distinctive character. These swarms are shown in Figs. 7 and 8.

The main distinction of the Cosmos 1375 group is the excellence of the correlation, the scatter being roughly half that seen in Cosmos 1275, for example. However, the median albedo (10%) is identical to that of the total population. The uniformity of albedo for the Cosmos 1375 swarm is only one of the peculiarities of this group. For example, there is remarkably little scatter in the inclinations and eccentricities of the orbits of the group, and the distribution in the right ascensions of the node show no definite central clump as do most other swarms. All these effects suggest a very low energy cause for the breakup.

Spot 1/Viking is peculiar primarily because all objects with optical diameters greater than 20 cm have albedos in excess of 17% (and a median albedo of 24%), whereas all objects with diameters less than 20 cm have albedos less than 10%. The unusually high albedos of the larger objects confirm the earlier finding of Potter et al.[1] that albedos for Spot1/Viking objects are roughly twice those of other swarms. It is tempting to speculate that such differences might be related to the cause of the fragmention, but, as yet, there is too little information to draw any conclusions.

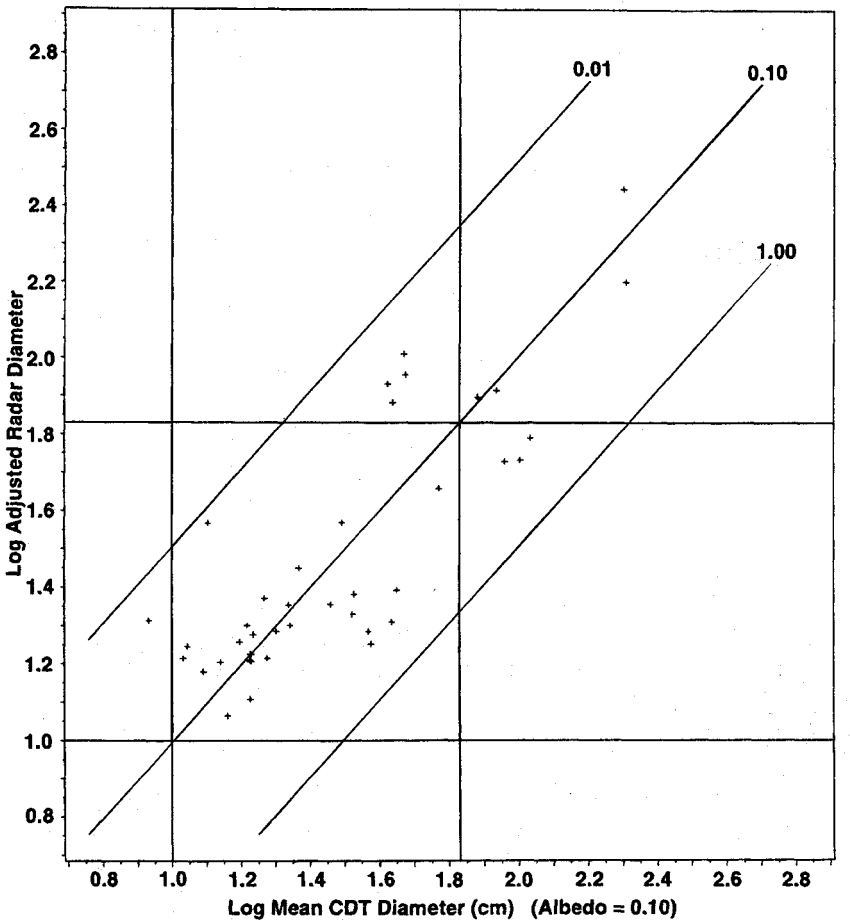

Fig. 6 Optical vs radar diams for 40 objects with well-determined phase functions.

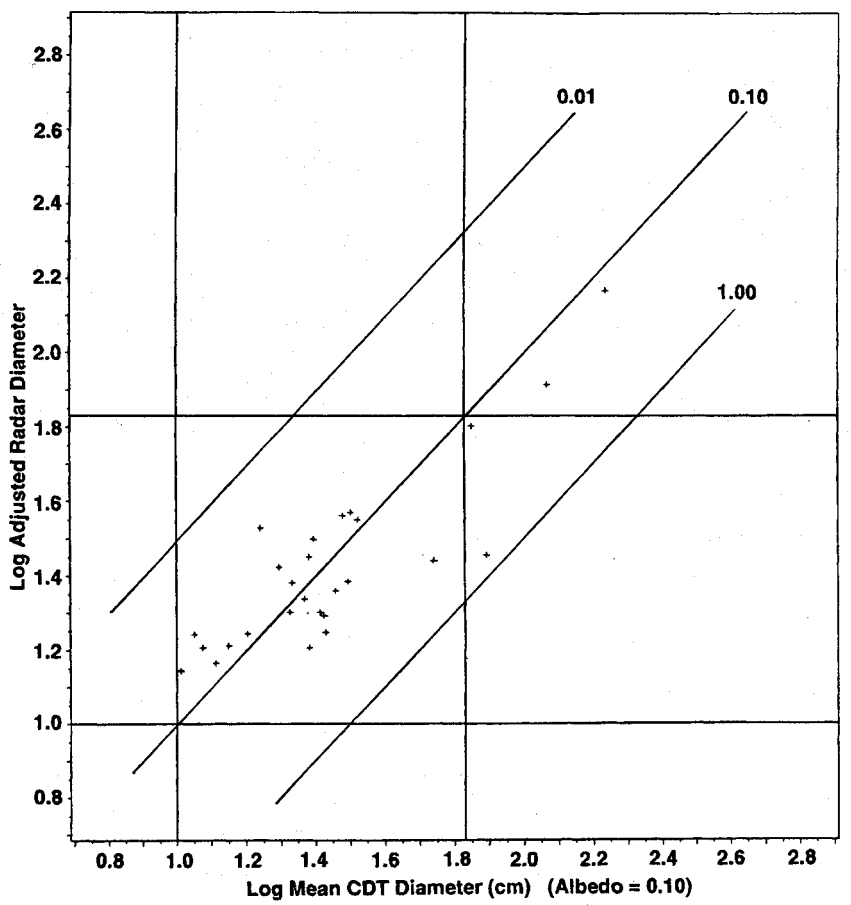

Fig. 7 Optical vs radar diams for Cosmos 1375 debris.

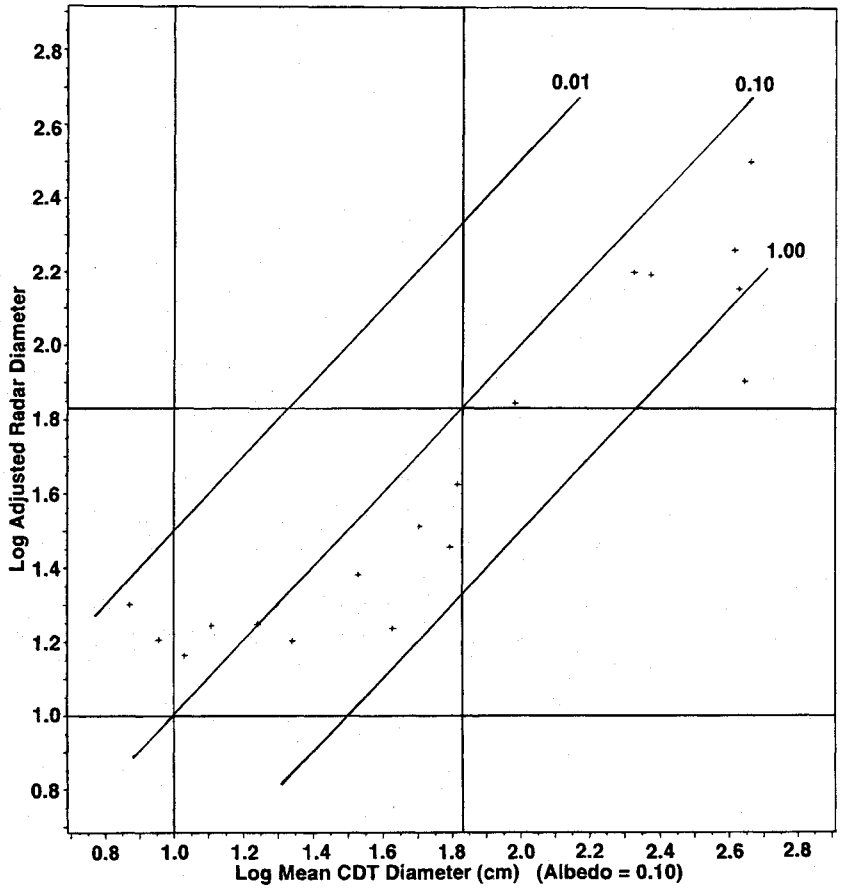

Fig. 8 Optical vs radar diams for Spot 1/Viking debris.

The horizontal tail of objects with optical diameters less than 20 cm is noteworthy but puzzling. This is similar to the "veer slightly to the left" seen in the total population that was discussed in a previous section. There, the somewhat larger scatter in the data suggested the effect was probably due to the nearby cutoff in the radar data. In this case the reduced scatter makes this explanation more difficult to accept and strongly suggests that the objects with diameters less than 20 cm are indeed darker. However, more extensive data would be highly desirable before reaching any firm conclusions.

Acknowledgments

We wish to thank Andrew E. Potter, Branch Chief of the JSC Space Sciences Branch, for his enthusiastic support of this project both financially and technically. We are also grateful to colleagues Donald J. Kessler and Herbert A. Zook for frequent technical discussions. We wish to acknowledge the substantial contributions of Barbara S. Nowakowski, David L. Talent, and Jerry L. Winkler, all with Lockheed Engineering and Sciences Company. The hospitality of the staff of the Rattlesnake Mountain Observatory of the Battelle Pacific Northwest Laboratories is also greatly appreciated.

References

[1] Potter, A. E., Henize, K. G., and Talent, D. L., "Albedo Estimates for Debris," *Orbital Debris from Upper-Stage Breakup*, edited by J. P. Loftus Jr., Vol. 121, Progress in Astronautics and Aeronautics, AIAA, Washington, DC, 1989, pp. 147–156.

[2] Henize, K. G., and Stanley, J. F., "Optical Observations of Space Debris," AIAA Paper 90-1340, April 1990.

[3] Lebofsky, L. A., and Vilas, F., "Thermal Models Applicable for Visual and Infrared Studies of Orbital Debris," *Advances in Space Research*, Vol. 10, Nos. 3–4, 1990, pp. (3)377–(3)380.

[4] Lambert, J. V., Osteen, T. J., and Kraszewski, W. A., "Determination of Debris Albedo from Visible and Infrared Brightnesses," Society of Photo-Optical Instrumentation Engineers, SPIE Paper 1951-04, April 1993.

[5] Henize, K. G., O'Neill, C. A., and Mulrooney, M. K., "CCD Observations of Orbital Debris," AIAA Paper 90-3870, Sept. 1990.

[6] Allen, C. W., "Photometry of Planets and Satellites," England, UK, *Astrophysical Quantities*, 3rd ed., Athlone Press, London, 1976, p. 143.

[7] Henize, K. G., Anz-Meador, P. D., and Tracy, T. E., "A Study of Systematic Effects in Eglin (AN/FPS-85) RCS Data," *Proceedings of the 1993 Space Surveillance Workshop*, Lincoln Lab., Project Rept. STK-206, Vol. 1, April 1993, pp. 179–188.

[8] Badhwar, G. D., and Anz-Meador, P. D., "Determination of the Area and Mass Distribution of Orbital Debris Fragments," *Earth, Moon, and Planets*, Vol. 45, Kluwer Academic Publishers, Dordrecht, The Netherlands, 1989, pp. 29–51.

[9] Burns, W. S., "AN/FPS-85 Radar Cross-Section Calibration," Lincoln Lab., project Rept. STK-150, April 1990, pp. 1–27.

[10] Stansbery, E. G., Pitts, C. C., Bohannon, G., Zechar, C., Tracy, T., and Stanley, J. F., "Size and Orbit Analysis of Orbital Debris Data Collected Using the Haystack Radar," NASA JSC-25245, 1991.

Ronald K. Clark
Associate Editor